BJP British Journal of Pharmacology

DOI:10.1111/bph.12406
www.brjpharmacol.org

RESEARCH PAPER

# Preclinical evaluation of 4-[3,5-bis(2-chlorobenzylidene)-4-oxo-piperidine-1-yl]-4-oxo-2-butenoic acid, in a mouse model of lung cancer xenograft

Vivek R Yadav*, Kaustuv Sahoo* and Vibhudutta Awasthi

*Department of Pharmaceutical Sciences, University of Oklahoma Health Sciences Center, Oklahoma City, OK, USA*

**Correspondence**
Vibhudutta Awasthi, Department of Pharmaceutical Sciences, University of Oklahoma Health Sciences Center, CPB309, 1110 North Stonewall Avenue, Oklahoma City, OK 73117, USA.
E-mail: vawasthi@ouhsc.edu

*Vivek R Yadav and Kaustuv Sahoo contributed equally to this work.

**Keywords**
CLEFMA; NF-κB; lung cancer; angiogenesis; apoptosis

**Received**
23 May 2013
**Revised**
30 July 2013
**Accepted**
29 August 2013

## BACKGROUND AND PURPOSE

4-[3,5-Bis(2-chlorobenzylidene)-4-oxo-piperidine-1-yl]-4-oxo-2-butenoic acid CLEFMA is a new anti-cancer molecule. Here, we investigated changes in apoptosis and inflammatory markers during CLEFMA-induced tumour suppression.

## EXPERIMENTAL APPROACH

Lung adenocarcinoma H441 and A549, and normal lung fibroblast CCL151 cell lines were used, along with a xenograft model of H441 cells implanted in mice. Tumour tissues were analysed by immunoblotting, immunohistochemistry and/or biochemical assays. The *ex vivo* results were confirmed by performing selected assays in cultured cells.

## KEY RESULTS

CLEFMA-induced cell death was associated with cleavage of caspases 3/9 and PARP. *In vivo,* CLEFMA treatment resulted in a dose-dependent suppression of tumour growth and $^{18}$F-fluorodeoxyglucose uptake in tumours, along with a reduction in the expression of the proliferation marker Ki-67. In tumour tissue homogenates, the anti-apoptotic markers (cellular inhibitor of apoptosis protein-1(cIAP1), Bcl-xL, Bcl-2, and survivin) were inhibited and the pro-apoptotic Bax and BID were up-regulated. Further, CLEFMA decreased translocation of phospho-p65–NF-κB into the nucleus. *In vitro*, it inhibited the DNA-binding and transcriptional activity of NF-κB. It also reduced the expression of COX-2 in tumours and significantly depressed serum TNF-α and IL-6 levels. These effects of CLEFMA were accompanied by a reduced transcription and/or translation of the invasion markers VEGF, MMP9, MMP10, Cyclin D1 and ICAM-1.

## CONCLUSIONS AND IMPLICATIONS

Overall, CLEFMA inhibited growth of lung cancer xenografts and this tumour suppression was associated with NF-κB-regulated anti-inflammatory and anti-metastatic effects.

### Abbreviations

BrdU, bromodeoxyuridine; cIAP1, cellular inhibitor of apoptosis protein-1; CLEFMA, 4-[3,5-bis(2-chlorobenzylidene)-4-oxo-piperidine-1-yl]-4-oxo-2-butenoic acid; FDG, $^{18}$F-fluorodeoxyglucose; ICAM-1, intercellular adhesion molecule 1; IHC, immunohistochemical; IKK, inhibitor of NF-κB kinase; TMB, 3,3′,5,5′-tetramethylbenzidine

## Introduction

4-[3,5-Bis(2-chlorobenzylidene)-4-oxo-piperidine-1-yl]-4-oxo-2-butenoic acid (CLEFMA) is an anti-proliferative compound that is undergoing preclinical evaluation. Structurally, it resembles a broader group of chemicals that are categorized as chalcones with a diphenyldihaloketone core (Figure 1A). In earlier work, CLEFMA potently inhibited the viability of H441 lung adenocarcinoma cells by inducing autophagy-associated cell death (Lagisetty *et al.*, 2010; Sahoo *et al.*, 2012). A combination of gene expression profile, pathway analysis and biochemical assays led us to associate the

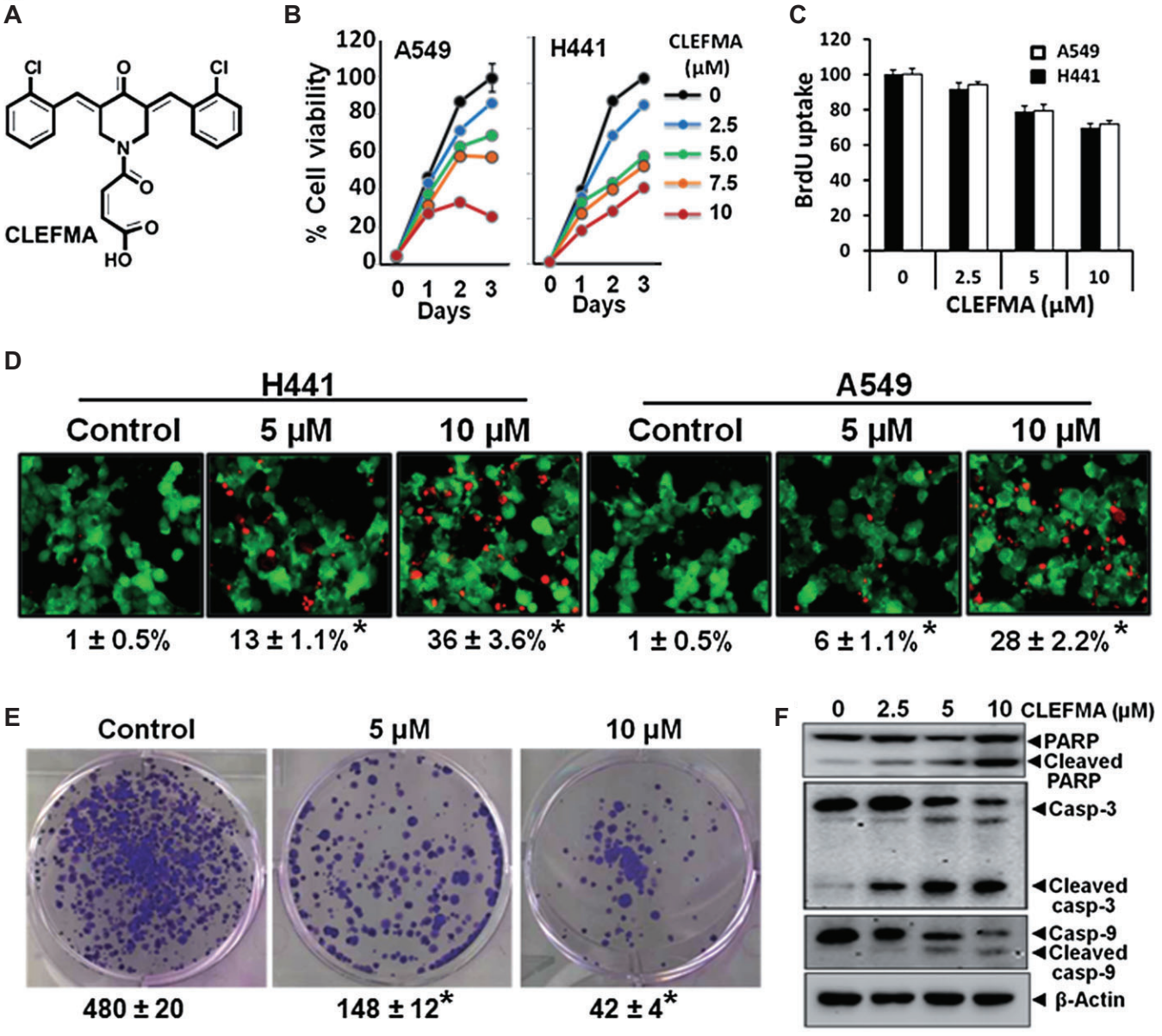


## Figure 1

CLEFMA inhibits cell viability and proliferation, and induces apoptosis in lung cancer cells *in vitro*. (A) The chemical structure of CLEFMA. (B) Dose-dependent suppression of percent cell viability [3-(4,5-dimethylthiazol-2-yl)-2,5-diphenyltetrazolium bromide assay] in lung cancer cell lines A549 and H441 (mean ± SEM, the error bars are too small to be seen). (C) The CLEFMA treatment for 48 h suppresses proliferation of A549 and H441 cells, as observed in BrdU uptake assay. (D) A confirmation of CLEFMA-induced cell death by fluorescence-based live/dead assay after CLEFMA treatment of cells for 24 h. The red fluorescence is the measure of number of dead cells, whereas the percentages indicate the proportion of dead cells. The data shown are representative of two independent experiments (*$P < 0.05$ compared with control). (E) CLEFMA suppressed the long-term colony formation in H441 cells. The colonies were stained with crystal violet and counted. Compared with the control H441 cells, the colony-forming ability of treated cells decreased to approximately 30 and 10% with 5 and 10 μM CLEFMA respectively. The values are mean ± SEM from three independent replicates (*$P < 0.05$ compared with control). (F) The treatment of H441 cells with CLEFMA for 24 h induced caspase activation and PARP cleavage. The whole-cell extracts were analysed by Western blotting with the indicated antibodies.

CLEFMA-induced anti-proliferative response with the phenotypic markers of oxidative stress (Sahoo *et al.*, 2012). In this report, we have evaluated tumour suppression in a mouse model of lung cancer, with the primary objective of examining the changes in key determinants of inflammation.

Inflammation is a precursor for many cancers (Karin *et al.*, 2006; Vendramini-Costa and Carvalho, 2012). It stimulates a rise in the levels of microRNA-155 that causes a drop in the levels of proteins involved in DNA repair, resulting in a higher rate of spontaneous gene mutations, which can lead to cancer (Tili *et al.*, 2011). Lung cancer is a classic example of inflammation-induced carcinogenesis. The lung is a unique organ by virtue of its functional anatomy – large surface area – and continuous exposure to inflammation-causing environmental toxins. It is established that pulmonary inflammation plays a role in initiation and promotion of lung cancer. A pivotal factor in inflammation and associated carcinogenesis is the transcription factor NF-κB (Chaturvedi *et al.*, 2011). It is a crucial regulator of inflammatory and immune responses, as well as cell survival (DiDonato *et al.*, 2012). Cancer cells are able to sustain NF-κB activation and recruit inflammatory cells, which helps cancer cells metastasize (Stathopoulos *et al.*, 2008; Kim *et al.*, 2009). The constitutively activated NF-κB prevents apoptosis in cancer cells and orchestrates a vicious cycle by stimulating the production of pro-inflammatory cytokines (Greten *et al.*, 2004; Pikarsky *et al.*, 2004). Therefore, NF-κB is an attractive target for cancer prevention and therapy in inflammation-associated cancer. A number of NF-κB inhibitors have been found useful, either alone or in combination with other drugs, for chemotherapy of lung cancer (Hoffmann *et al.*, 2007; Yadav *et al.*, 2012b).

As a potent diphenyldihaloketone analogue, CLEFMA is being developed as an anti-cancer agent on the basis of a comprehensive structure activity relationship study (Lagisetty *et al.*, 2010). Previously, we reported the efficacy of a liposome formulation of CLEFMA in a rat xenograft model, where we also noted that normal human lung fibroblasts were resistant to CLEFMA-induced cell death (Agashe *et al.*, 2011). Here, we evaluated the molecular effects of CLEFMA in a mouse preclinical xenograft model. Because molecules with similar structural features have been reported to affect the NF-κB pathway (Kasinski *et al.*, 2008), we specifically focused our attention on NF-κB and accompanying inflammatory, proliferative, invasive and angiogenic biomarkers. We chose the lung adenocarcinoma H441 xenograft model because of high chemoresistance, p53 as well as k-Ras mutation (Meylan *et al.*, 2009; Sunaga *et al.*, 2011), and high constitutive EGF/EGF receptor activation exhibited by these cells (Wu *et al.*, 2007).

## Methods

CLEFMA was synthesized in-house by the methods detailed elsewhere (Lagisetty *et al.*, 2010). Human non-small-cell lung cancer cell lines NCI-H441 and A549, and normal lung fibroblasts CCL151 were obtained from American Type Culture Collection (Manassas, VA, USA) and maintained at 37°C with 5% $CO_2$ in RPMI 1640 medium (Invitrogen, Carlsbad, CA, USA) supplemented with 10% FBS and 50 μg·mL$^{-1}$ gentamicin. The mouse monoclonal antibodies to survivin, BAX, BID, Bcl-xL and cellular inhibitor of apoptosis protein-1 (cIAP1) and the rabbit polyclonal antibody to Ki-67 and the goat polyclonal antibodies to MMP9 and COX-2 were supplied by Santa Cruz Biotechnology (Santa Cruz, CA, USA). Rabbit polyclonal antibodies to cleaved PARP, total PARP, caspase-3 and caspase-9 and the rabbit monoclonal antibodies to phospho-p65-NF-κB, Bcl-2; phospho-p53; phospho-IκBα; IκBα; phospho-IKKα/β; IKKβ; VEGF-2 and cyclin D1 and the mouse monoclonal antibody to CD31 were purchased from Cell Signaling Technology (Boston, MA, USA). Anti-β-actin antibody was obtained from Sigma-Aldrich (St. Louis, MO, USA). The secondary antibodies against IgG of various species were obtained from Santa Cruz Biotechnology. For gene silencing, IκBα small interfering (si)-RNA was obtained from Cell Signaling Technology.

### *Cell viability assays*

The effect of CLEFMA on cell viability of H441 and A549 cells was determined by 3-(4,5-dimethylthiazol-2-yl)-2,5-diphenyltetrazolium bromide assay, as previously described (Yadav *et al.*, 2012a). To further ascertain cell death, we used a Live/Dead assay kit from Marker Gene Technologies Inc. (Eugene, OR, USA) according to the manufacturer's instructions. The cells were analysed under a type DM4000B fluorescence microscope (Leica, Buffalo Grove, IL, USA).

Cancer cell proliferation was investigated by ELISA for the incorporation of bromodeoxyuridine (BrdU) into DNA. Briefly, the cells were treated with CLEFMA for 48 h and labelled with BrdU (1:100; Life Technologies, Grand Island, NY, USA) for 12 h at 37°C. The cells were fixed in 70% alcohol and incubated with mouse HRP-conjugated anti-BrdU peroxidase antibody solution (1:1000) for 90 min. The colour was developed with 3,3′,5,5′-tetramethylbenzidine (TMB; Sigma, St. Louis, MO, USA) substrate for 20 min, and the reaction was stopped by addition of 50 μL of 1 M $H_2SO_4$. The incorporation of BrdU was quantified by measuring the absorbance at 450 nm.

### *Clonogenic assay*

H441 cells were grown in 100 mm Petri dishes and treated with CLEFMA (10 μM) for 24 h. The cells were re-plated at a density of 500 cells per well in 35 mm dishes (3 per group) and incubated for 10 days. The colonies were stained with 0.3% crystal violet solution (1:1 methanol and $H_2O$) and counted. Each data point was calculated as a mean of three replicate wells.

### *Cell cycle analyses*

H441 cells were treated with CLEFMA (10 μM) for 48–72 h. Single-cell suspensions were fixed using 70% ethanol for 2 h, before permeabilizing the cells with 0.1% Triton X-100 (Sigma-Aldrich), followed by staining with 1 mg·mL$^{-1}$ propidium iodide (Sigma-Aldrich) in 200 μg·mL$^{-1}$ DNase-free RNase (Sigma-Aldrich). Flow cytometry was performed on a FACSCalibur analyser (Becton Dickinson, Mountain View, CA, USA) by capturing 50 000 events per sample. The results were analysed with ModFit LT™ software (Verity Software House, Topsham, ME, USA).

## NF-κB DNA-binding and luciferase reporter assays

The effect of CLEFMA on NF-κB p65-DNA interaction was assessed in the nuclear fraction of H441 cells by TransAM NF-κB p65 kit according to the manufacturer's instructions (Active Motif, Carlsbad, CA, USA). A specific NF-κB inhibitor, BAY 11-7082 (Cayman Chemical, Ann Arbor, MI, USA), was used at 10 μM as a positive control. To confirm the results from NF-κB DNA-binding assay, we performed a standard NF-κB activity assay based on a luciferase reporter. Briefly, H441 cells were transfected with the NF-κB firefly luciferase reporter plasmid pGL4.32 [luc2P/NF-κB-RE/Hygro, Promega, Madison, WI, USA; kindly provided by Dr. Kelly Standifer, University of Oklahoma Health Sciences Center (OUHSC)]. For ensuring successful transfection, the control wells of H441 cells were transfected with a plasmid DNA construct expressing enhanced green fluorescent protein (pHYG-EGFP; Clontech, Mountain View, CA, USA) and observed under Leica DM4000B fluorescent microscope. The luciferase activity was measured by using the Dual-Luciferase Assay System (Promega) and normalized to protein concentration.

## Mouse model of human lung cancer xenograft

All animal care and experimental protocols were reviewed and approved by the Institutional Animal Care and Use Committee at the OUHSC. All studies involving animals are reported in accordance with the ARRIVE guidelines for reporting experiments involving animals (Kilkenny *et al.*, 2010; McGrath *et al.*, 2010). A total of 6 animals per group were used in the experiments described here. Male athymic nu/nu mice (4 weeks old) were obtained from the breeding colony of Harlan Laboratories (Indianapolis, IN, USA). Before initiating the experiment, we allowed the mice to acclimatize for at least 5 days. For xenograft implantation, H441 cells were harvested, washed in serum-free medium and resuspended in 0.1 M PBS (pH 7.2). A single-cell suspension with >90% viability was used for subcutaneous injections in mice ($2 \times 10^6$ cells per implant).

## Drug treatment

After allowing 1.5 weeks of tumour growth, the mice were randomly assigned to one of the following treatment groups ($n$ = 6 each): (i) vehicle control; (ii) CLEFMA low dose (0.2 mg·kg$^{-1}$); and (iii) CLEFMA high dose (0.4 mg·kg$^{-1}$). The maximum cumulative dose of CLEFMA over 4 weeks of treatment was 11.2 mg·kg$^{-1}$. The treatments were administered i.p. on a daily basis. The tumour volumes (long diameter × short diameter$^2$ × 0.52) and body weights were measured every week for up to 4 weeks. Upon killing, blood was collected by cardiac puncture; serum was separated and stored at –80°C. The excised tumours were divided into two parts. The first part was formalin-fixed and paraffin-embedded for haematoxylin and eosin and immunohistochemical (IHC) staining at Oklahoma Medical Research Foundation's Imaging Core Facility, Oklahoma City, OK, USA. The second part was snap-frozen in liquid nitrogen and stored at –80°C.

## PET

After 28 days of treatment, the animals were recruited for PET, using $^{18}$F-fluorodeoxyglucose (FDG) as a biomarker of tumour growth. PET imaging was performed at the Research Imaging Facility, OUHSC-College of Pharmacy. FDG (100 μCi, 0.1 mL) was injected into the tail vein of anaesthetized mice (2–3% isoflurane in oxygen). After 2 h, the animals were anaesthetized again and placed inside the PET detector of a X-O-PET machine (Gamma Medica-Ideas, Northridge, CA, USA). Static images of FDG accumulation were acquired for 20 min, followed by a fly-mode CT. The PET image was reconstructed using a filtered back projection algorithm and fused with the CT image to create a composite PET/CT image.

## Nuclear extract from tumour tissue

The tumour tissues (75–100 mg per mouse) were minced and incubated on ice for 30 min in 0.5 mL of an ice-cold buffer consisting of 10 mM HEPES (pH 7.9), 1.5 mM KCl, 10 mM $MgCl_2$, 0.5 mM DTT, 0.1% IGEPAL CA-630 and 0.5 mM PMSF. The minced tissues were homogenized using a Dounce homogenizer and centrifuged at 16 000× $g$ for 10 min at 4°C. The resulting nuclear pellets were suspended in 0.2 mL of a buffer consisting of 20 mM HEPES (pH 7.9), 25% glycerol, 1.5 mM $MgCl_2$, 420 mM NaCl, 0.5 mM DTT, 0.2 mM EDTA, 0.5 mM PMSF and 2 μg·mL$^{-1}$ leupeptin. After allowing the suspensions to incubate on ice for 2 h with intermittent mixing, they were centrifuged at 16 000× $g$ at 4°C for 30 min. The supernatants (nuclear extracts) were collected for immunoblotting as described below.

## Western blot analysis of cancer biomarkers

The CLEFMA-treated cells and minced tumour tissues (75–100 mg per mouse) were incubated on ice for 30 min in 0.5 mL of ice-cold lysate buffer consisting of 10% NP-40, 5 M NaCl, 1 M HEPES, 0.1 M EGTA, 0.5 M EDTA, 0.1 M PMSF, 0.2 M sodium orthovanadate, 1 M NaF, 2 μg·mL$^{-1}$ aprotinin and 2 μg·mL$^{-1}$ leupeptin. The protein was extracted by homogenization using a Dounce homogenizer and centrifugation at 16 000× $g$ at 4°C for 10 min. The proteins were fractionated by SDS-PAGE, electrotransferred onto nitrocellulose membranes and blotted with respective primary antibodies, followed by an HRP-conjugated secondary antibody. The final detection was performed by enhanced chemiluminescence SuperSignal West Femto reagent (Thermo Scientific, Rockford, IL, USA).

## COX-2 activity assay

The activity of COX-2 in lysates of tumour xenografts in mice was estimated using a commercially available fluorescent activity assay kit (Cayman Chemical Company). The manufacturer's instructions provided with the kit were followed.

## Cytokine ELISA

The TNF-α levels were measured in serum by ELISA according to the method published earlier (Awasthi *et al.*, 2011). Briefly, the wells of Immulon 4 HBX plate (Thermo Electron Corporation, Milford, MA, USA) were coated overnight at 4°C, with 100 μL of 10 μg·mL$^{-1}$ purified rat anti-mouse TNF-α antibody (BD Biosciences, San Jose, Ca, USA). After the prescribed washing steps, the wells were blocked at room temperature for 2 h with 3% BSA, followed by washing with PBS 0.02% Tween 20 (Sigma-Aldrich). To the wells, 100 μL of cytokine standard solutions, or suitably diluted samples of cell-free supernatant,

were added. The dilutions of the samples, standards and antibodies were prepared in 3% BSA-PBS. After overnight incubation at 4°C, the wells were washed and incubated for 2 h at room temperature with 100 µL of 2.5 µg·mL$^{-1}$ of biotin-labelled anti-mouse IgG antibody (BD Biosciences), and incubated. Following another washing, 100 µL of 1:200 diluted streptavidin-HRP (BD Biosciences) was added and the plate was incubated for 1 h at room temperature. After a final wash, 100 µL of TMB substrate solution was added. The reaction was stopped after 15 min, and the plate was read at 450 nm using a BioTek 96-well multiscanner (Winooski, VT, USA).

The IL-6 levels were measured in a manner similar to that described for TNF-α using the rat anti-mouse IL-6 ELISA set (SouthernBiotech, Birmingham, AL, USA). The manufacturer's instructions provided with the kit were followed.

### *RNA extraction and real-time PCR*

The total RNA was extracted from approximately 100 mg of tumour tissue using RNA-STAT60 (Tel-Test Inc., Friendswood, TX, USA) and quantified by absorbance values at 260 nm. The reverse transcriptase reaction was performed for 1 h at 42°C using 2 µg of total RNA, 1 µg of oligo(dT), 200 U of M-MLV reverse transcriptase enzyme, 500 µM dNTP mix and 25 U of RNase inhibitor (Promega). The resultant cDNA was used to carry out 40 PCR cycles consisting of 15 s at 95°C, 30 s at 58°C and 30 s at 72°C on an ABI Prism 7000 sequence detection system (Applied Biosystems, Foster City, CA, USA). The reactions were performed using SYBR Green II (Qiagen, Valencia, CA, USA) and GoTaq colourless master mix (Promega) (Vilekar *et al.*, 2012). Each PCR was set up in triplicate wells in a total volume of 25 µL. The reaction mixture contained the cDNA equivalent of 20 ng total RNA. The quantitative values of the genes of interest were normalized using β-actin as the endogenous reference, and fold-increase over control values was calculated using the relative quantification method of $2^{-\Delta\Delta}$ $C_t$. All the primers were of 20 base pairs (Table 1).

### *Immunohistochemistry*

The formaldehyde-fixed and paraffin-embedded tumour samples were processed according to standard procedures. Briefly, the thin sections of tumour tissue were sequentially delipidated in xylene, ethanol and PBS. After washing in PBS, the slides were blocked with a protein block solution (Dako-Cytomation, Carpinteria, CA, USA) for 20 min and incubated overnight with anti-human phospho-p65 (1:200), COX-2 (1:50), MMP9 (1:50), Cyclin D1 (1:500), VEGF (1:500), Ki-67 (1:250) and CD31 (1:200) antibodies. The slides were washed and incubated with biotinylated link universal anti-serum, followed by HRP streptavidin conjugate. The slides were rinsed and the colour was developed using 3,3′-diaminobenzidine hydrochloride as a chromogen. Finally, the sections were counterstained with Mayer's haematoxylin solution and mounted with DPX mounting medium for evaluation. The sections were observed with an Olympus microscope IX701, and digital computer images were recorded using an Olympus DP70 camera (Olympus America, Center Valley, PA, USA).

**Table 1**

Human primers for RT-PCR experiments obtained from Real Time Primers or Integrated DNA Technologies

| | |
|---|---|
| ICAM-1[a] | Forward 5′-TTT TCT ATC GGC ACA AAA GC-3′<br>Reverse 5′-AAT GCA AAC AGG ACA AGA GG-3′ |
| MMP9[a] | Forward 5′-CTC TGG AGG TTC GAC GTG-3′<br>Reverse 5′-GTC CAC CTG GTT CAA CTC AC-3′ |
| MMP10[a] | Forward 5′-GCC CAC AAA ATC TGT TCC TT-3′<br>Reverse 5′-ATT CAG GTT CAG GGT TCC AG-3′ |
| VEGF-A[a] | Forward 5′-AGA CAC ACC CAC CCA CAT AC-3′<br>Reverse 5′-TGC CAG AGT CTC TCA TCT CC-3′ |
| NFKB1[a] | Forward 5′-GAA GCT GAA GTG CAT CCA AA-3′<br>Reverse 5′-GGG ACA ACA GCA ATG ACA AC-3′ |
| COX-2[b] | Forward 5′-TCA AAT GAG ATT GTG GGA AAA TTG-3′<br>Reverse 5′-TCT AGT AGA GAC GGA CTC ATA GAA-3′ |

[a]Real Time Primers (Elkins Park, PA, USA).
[b]Integrated DNA Technologies (Coralville, IA, USA).

### *Data analysis*

The statistical comparisons between drug-treated and untreated groups were performed using Prism 5.0 (GraphPad Software, Inc., La Jolla, CA, USA). The raw data were subjected to ANOVA. The results were presented as means ± SD. *P*-value of <0.05 was considered statistically significant. For PET data, the fused images were employed for visualization and analysis using Amira 3.1 software (Visage Image Inc., San Diego, CA, USA). The regions of interest were drawn around the tumour CT volume, and the amount of radioactivity signal was normalized by the injected dose per g body weight. The standard uptake values were expressed as counts·µCi$^{-1}$·g$^{-1}$ body weight. The immunoblotting and IHC results are representative of three separate analyses.

## Results

The goal of this study was to investigate the apoptotic mode of cell death and the molecular entities involved in the suppression of lung tumour growth by CLEFMA. The chemical structure of CLEFMA is provided in Figure 1A. We employed assays for selective biomarkers of inflammation, angiogenesis, cell survival, cell proliferation and invasion in tumour tissues from a xenograft mouse model.

### *CLEFMA induces apoptosis in lung cancer cells*

CLEFMA inhibited the viability and proliferation of H441 and A549 cells *in vitro* in a dose-dependent manner (Figure 1B,C). The $IC_{50}$ values for CLEFMA were 6.4 µM in H441 cells and 8.9 µM in A549 cells. The induction of cell death by CLEFMA was confirmed by a fluorescence-based assay of live and dead cells (Figure 1D). CLEFMA treatment also significantly suppressed the colony-forming ability of H441 cells (Figure 1E). Further, CLEFMA treatment resulted in the accumulation of cleaved PARP, caspase-3 and caspase-9 in a dose-dependent manner (Figure 1F). These results suggest that CLEFMA decreased the viability of cancer cells and induced cell death by activating a caspase-dependent apoptotic pathway.

### *CLEFMA inhibits tumour growth in a xenograft mouse model*

After establishing the *in vitro* evidence of CLEFMA-induced apoptosis, we designed studies in mice to determine whether

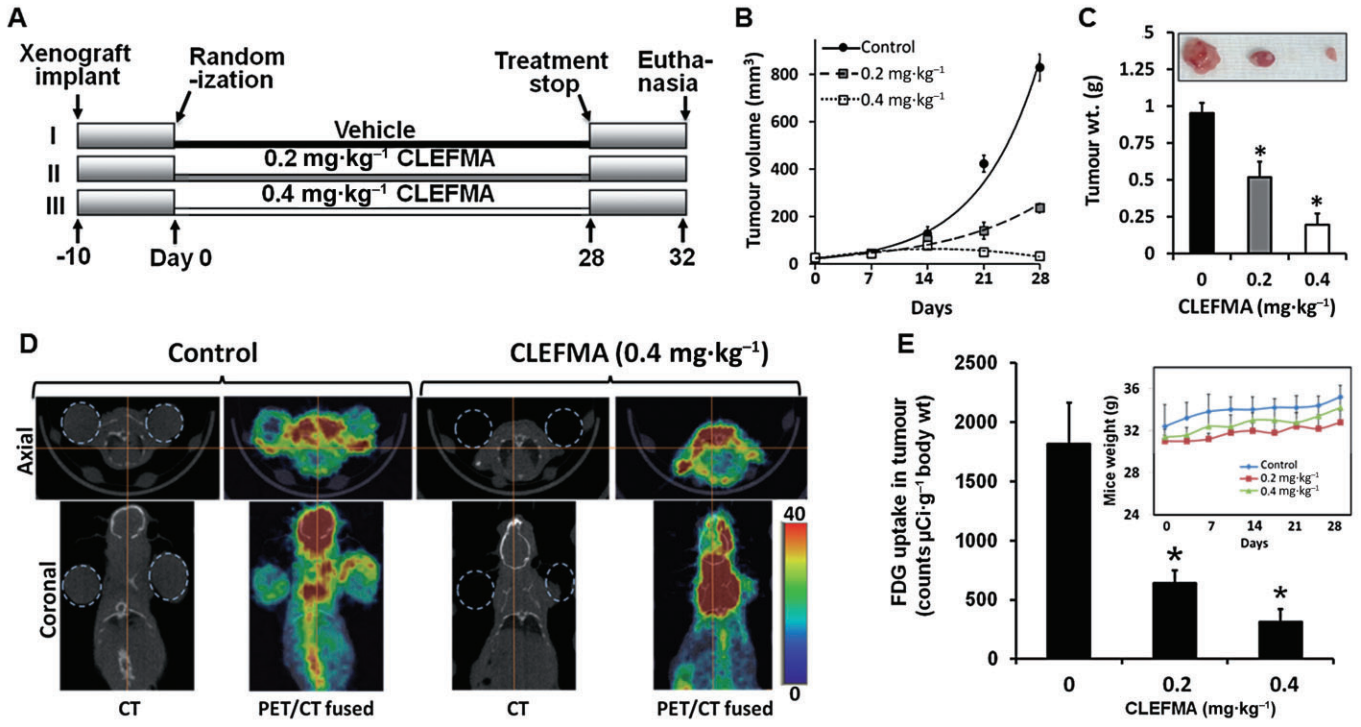


## Figure 2

CLEFMA suppresses growth of H441 xenograft tumours in nude mice. (A) An outline of the treatment protocol used. Group I was injected with vehicle (50 µL), whereas group II and group III received 0.2 and 0.4 mg·kg$^{-1}$ of CLEFMA, respectively, in 50 µL volume. The injections were performed i.p. on a daily basis. (B) The tumour volumes (mean ± SEM) at various times after initiation of CLEFMA treatment ($n = 6$). The 24 and 28 day values from CLEFMA-treated groups were significantly different from the control group; $P < 0.05$. (C) The tumour weights at necropsy of the mice on day 32 (mean ± SEM); the inset shows pictographs of the excised tumours. *$P < 0.05$, significantly different from untreated tumours. (D) CLEFMA reduced the uptake of FDG in tumour. PET/CT was performed after 28 days of treatment initiation. A representative set of axial and coronal PET/CT images of FDG accumulation in control and treated mice is shown. The tumour volume is depicted by encircled regions of interest. (E) A quantitative analysis of FDG uptake in tumour voxels was performed and the amount of radioactivity signal in the voxels was normalized by the injected dose per gram body weight (counts·µCi$^{-1}$·g$^{-1}$; *$P < 0.05$ significantly different from untreated tumours. The inset shows that CLEFMA administration over 4 weeks does not alter the body weight of mice.

CLEFMA inhibited tumour growth *in vivo*. The treatment was started 10 days after tumour implantation and lasted for 4 weeks (Figure 2A). The average tumour volume at the time of randomization was 54 ± 8.4 mm$^3$. We found a more rapid increase in tumour volume in the vehicle group as compared with that in the two treatment groups (Figure 2B). The average tumour volume in the control mice increased to 828 ± 57 mm$^3$. In comparison, the average tumour volumes in the CLEFMA-treated groups were 236 ± 12 mm$^3$ and 32 ± 8.5 mm$^3$ for 0.2 and 0.4 mg·kg$^{-1}$ doses respectively. Thus, the percentage of tumour inhibition for a CLEFMA dose of 0.4 mg·kg$^{-1}$ was approximately 96%. The observations were confirmed by tumour weights at necropsy (Figure 2C).

### *CLEFMA suppressed the uptake of FDG in tumour tissue*

To investigate the effect of CLEFMA on the metabolic turnover in tumour tissue, we performed PET using FDG as a biomarker of glucose metabolism. As shown in a representative picture (Figure 2D), the mice treated with vehicle control accumulated significant amounts of FDG in tumour, but the mice treated with CLEFMA showed negligible FDG uptake in tumour. Because of the complete suppression of tumour growth in mice receiving 0.4 mg·kg$^{-1}$ CLEFMA, the CT images could not delineate tumour voxels in this group. The same interpretation was drawn when the images were quantitatively analysed for FDG uptake in the tumour (Figure 2E). Compared with the control group of mice, the standard uptake value of FDG was reduced by 65 and 83% in the two CLEFMA-treated groups respectively. These results suggest that CLEFMA potently suppressed tumour growth *in vivo* with concomitant reductions in metabolic requirement in the tumour tissue.

### *CLEFMA induces apoptosis in tumours*

Next, we analysed the excised tumour tissues for biochemical markers of apoptotic cell death. Figure 3A shows that CLEFMA down-regulated the expression of anti-apoptotic markers cIAP1, Bcl-xL, Bcl-2 and survivin in tumours. At the same time, CLEFMA treatment induced the cleavage of pro-apoptotic protein BID and the expression of pro-apoptotic BAX in tumour tissue (Figure 3B). We also found that immunoreactive Ki-67, a specific cellular marker of proliferation, was unequivocally reduced by CLEFMA (Figure 3C). We

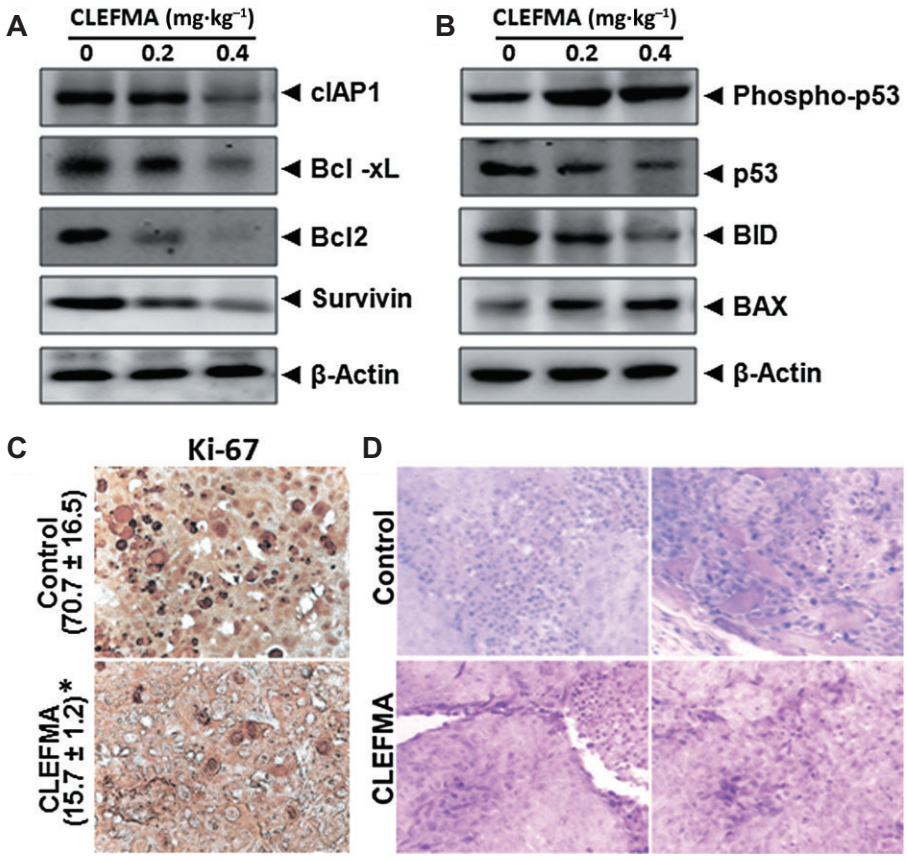


## Figure 3

CLEFMA suppresses anti-apoptotic genes and induces apoptosis in tumour tissue. (A) CLEFMA inhibited the expression of anti-apoptotic gene products, such as cIAP1, Bcl-xL, Bcl-2 and survivin. (B) CLEFMA treatment cleaved the BID protein and induced the expression of pro-apoptotic BAX in tumour tissue. (C) IHC analyses of proliferation marker Ki-67 indicated that the H441 tumour cell proliferation was inhibited in mice treated with CLEFMA (0.4 mg·kg$^{-1}$). The IHC values are represented as the mean ± SEM from three tumours per group. *$P < 0.05$ significantly different from untreated tumours. The tumours were selected randomly from each group. (D) Representative micrographs of H&E stained tumour tissue at 400× magnification. Two views each of a control tumour and a CLEFMA-treated tumour are shown.

then examined the microscopic morphology of tumours (Figure 3D). We observed a large infiltration of inflammatory cells, with densely cellular and mitotic figures visible in the control tumours. A few areas of necrotic disintegration were also seen. In comparison, the CLEFMA-treated tumour was histologically different and characterized by reduced infiltration of granulocytes and generalized lack of normal tissue integrity. There were many apoptotic cells in the CLEFMA group, whereas in the control groups, there were more tumour cells with apparently enlarged nuclei (Figure 3D).

### *CLEFMA inhibits NF-κB (p65) and associated signalling*

The treatment of mice with CLEFMA reduced the *NFkB1* gene transcripts in the xenografts, but the reduction was significant only at the higher dose 0.4 mg·kg$^{-1}$ (Figure 4A). Immunoblotting of the nuclear extracts of tumour tissues demonstrated that CLEFMA significantly reduced the nuclear levels of the phospho-p65 subunit (Figure 4B). The IHC analyses for phospho-p65 subunit indicated that the global amounts of phosphorylated NF-κB were significantly lower in the CLEFMA-treated tumours than in the control tumours (Figure 4C). The inhibitory effect of CLEFMA on NF-κB activity was confirmed in H441 cells *in vitro* (Figure 5). The effect of CLEFMA on DNA binding of NF-κB was dose dependent (Figure 5A). We further assayed the transcriptional activity of NF-κB by luciferase reporter assay and found that the CLEFMA treatment reduced NF-κB activity in H441 cells (Figure 5B). Notably, no significant inhibition of NF-κB DNA-binding activity was observed in normal lung fibroblasts CCL151, after treatment with CLEFMA (Figure 5C).

NF-κB activation and inhibition is usually observed together with changes in expression and/or phosphorylation of IκBα and the associated kinase IKKβ. We explored this phenomenon *in vitro* in CLEFMA-treated H441 cells (Figure 5D). As shown in Figure 5D, we found that CLEFMA increased the phosphorylation of IκBα, even when the total expression was not altered. An attempt to silence IκBα expression with si-RNA resulted in its partial suppression, but the effect of CLEFMA on phosphorylation levels remained intact. The corresponding effect of CLEFMA on the cell viability of H441 cells was also not affected by IκBα gene silencing

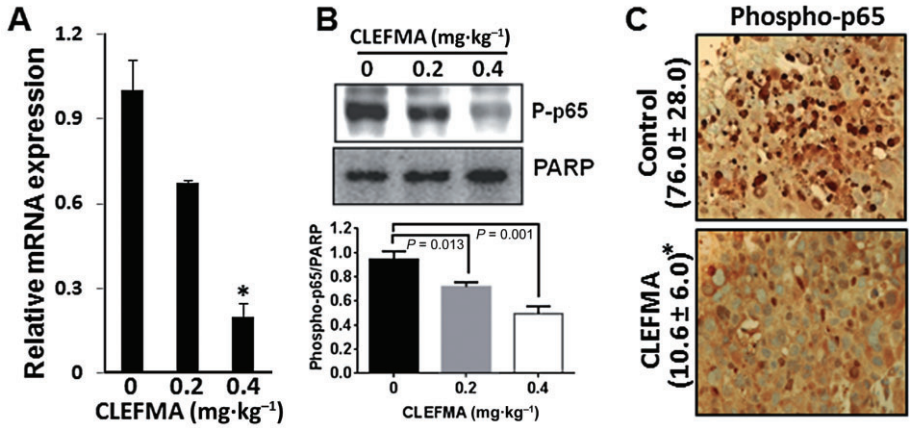


## Figure 4

CLEFMA suppresses NF-κB expression. (A) The treatment of mice with CLEFMA reduced the NF-κB mRNA expression in the tumour tissue. *$P < 0.05$ significantly different from untreated tumours. (B) A representative immunoblot of three sets showing that CLEFMA inhibited the nuclear translocation of phosphorylated-p65 in tumour tissue. Nuclear PARP was probed as a protein loading control. A densitometry of p65 immunoreactive bands normalized with PARP is shown in the lower panel. (C) A reduction in the phospho-p65 positivity in the IHC analyses of tumour tissues confirmed the inhibition of NF-κB by CLEFMA (0.4 mg·kg$^{-1}$). The IHC values (mean ± SEM) are indicative of positive staining of the antigen. *$P < 0.05$ significantly different from untreated tumours. At least three tissues from each group were selected randomly for reverse transcription PCR, immunoblotting and IHC.

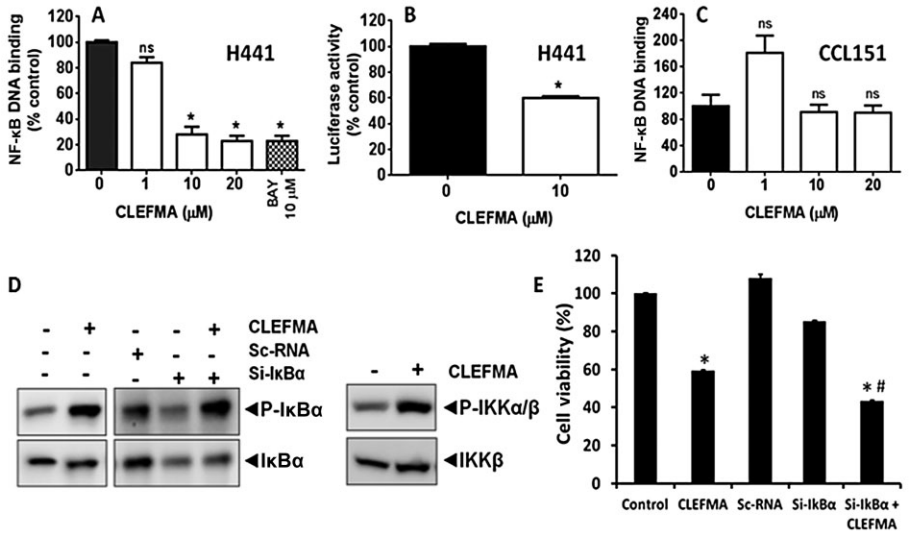


## Figure 5

CLEFMA inhibits NF-κB *in vitro*. (A) CLEFMA treatment reduced the DNA-binding activity of NF-κB in H441 cells *in vitro* in a dose-dependent manner. BAY 11-7082 is a specific NF-κB inhibitor and was used as a positive control. *$P < 0.05$ significantly different from untreated cells. (B) The suppressive effect of CLEFMA on NF-κB activity was further confirmed by a decrease in transcriptional NF-κB activity in a luciferase reporter assay (*$P < 0.05$ vs. untreated cells). (C) CLEFMA did not affect the NF-κB DNA-binding activity in normal lung fibroblasts CCL151. (D) CLEFMA reduced the degradation of IκBα. H441 cells were transfected with IκBα si-RNA using Fugene HD reagent. After 48 h of transfection, the cells were treated with 10 μM of CLEFMA for 12 h. (E) The cell viability studies in CLEFMA-treated H441 cells previously transfected with IκBα si-RNA. *$P < 0.05$ significantly different from control; #$P < 0.05$ significantly different from CLEFMA). Scrambled RNA was used as a control. All the *in vitro* assays were performed in triplicate.

(Figure 5E). These observed effects of CLEFMA on phosphorylation levels of IκBα are contrary to those of most NF-κB inhibitors. Because IκBα is a substrate for the IKKs, we studied the expression levels of its purportedly active form, phospho-IKKα/β. Again, we found that the phosphorylation of IKKα/β was enhanced by CLEFMA treatment, without accompanying changes in the total IKKβ expression (Figure 5D).

Some part of the effects of NF-κB on tumour survival is mediated through increased expression of COX-2 (Yadav *et al.*, 2012b). By immunoblotting and IHC analysis, we

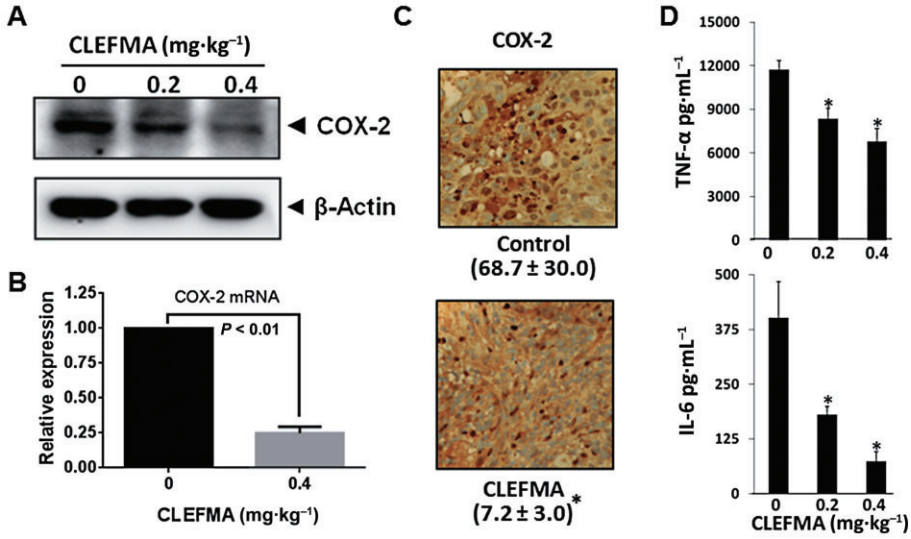


## Figure 6

CLEFMA suppresses COX-2 expression in tumours and reduces the serum levels of IL-6 and TNF-α. (A) CLEFMA inhibited the expression of COX-2 protein in tumour tissue. (B) The treatment with CLEFMA reduced the mRNA expression of COX-2 in tumour tissues. The tumour tissues from three mice each from control and treated (CLEFMA 0.4 mg·kg$^{-1}$) groups were processed for RT-PCR. *$P$ < 0.01 significantly different from untreated tumours. (C) IHC analyses of COX-2 in the tumour tissues confirmed its suppression by CLEFMA. The IHC values (mean ± SEM) are indicative of positive staining of the antigen. *$P$ < 0.05 significantly different from control. (D) The levels of IL-6 and TNF-α were detected by ELISA in serum of mice treated with CLEFMA or vehicle control. The values are mean ± SEM from three independent replicates (*$P$ < 0.05 significantly different from untreated mice. At least three tissues from each group were selected randomly for RT-PCR, immunoblotting and IHC; the cytokines in the serum samples ($n$ = 5) were estimated in triplicate.

found that CLEFMA inhibited COX-2 expression in the tumour tissues (Figure 6A,C respectively). That the COX-2 expression was also regulated at transcriptional level was deduced from the observation that CLEFMA decreased COX-2 mRNA levels (Figure 6B).

Two major effector molecules in the proinflammatory NF-κB pathway are the cytokines TNF-α and IL-6. Compared with the control animals, the levels of IL-6 and TNF-α in serum were significantly suppressed by CLEFMA in both treated groups (Figure 6D). The suppressive effect of CLEFMA on IL-6 was more marked than that on TNF-α. Overall, these observations in tumour tissues demonstrate the anti-inflammatory properties of CLEFMA, as expressed *in vivo*.

### *CLEFMA down-regulates the expression of NF-κB-regulated gene products*

NF-κB participates in the survival of tumour through regulation of mediators of invasion, such as ICAM-1, MMP9 and MMP10 and of angiogenesis (VEGF) (Himelstein *et al.*, 1994; Ferrara, 2002). Treatment with CLEFMA reduced the expression of VEGF, MMP9, MMP10 and ICAM-1 in tumour tissues at transcriptional level (Figure 7A). By immunoblotting, we found that the protein expression levels of cyclin D1, MMP9 and VEGF were also significantly reduced in tumours from CLEFMA-treated groups (Figure 7B). The changes in these proteins were confirmed by IHC assays (Figure 7C). Additionally, the expression of CD31 (a marker for angiogenesis and microvessel density) was also reduced by CLEFMA (Figure 7C). The cell cycle analyses of H441 cells *in vitro* revealed that CLEFMA-treated cells were arrested in S phase, which is compatible with the observation that CLEFMA reduced cyclin D1 expression *in vivo* (Figure 8).

## Discussion

CLEFMA is a novel molecule with a unique mechanistic basis of anti-proliferative activity (Lagisetty *et al.*, 2010). Earlier, we showed that it selectively modulates redox homeostasis in lung adenocarcinoma H441 cells but does not cause such alterations in normal lung fibroblasts (Sahoo *et al.*, 2012). In this report, we provide *in vivo* evidence of CLEFMA-induced inhibition of mediators of inflammation, cell proliferation, cell survival, invasion, angiogenesis and induction of apoptotic cell death in H441 xenografts. The first indication that CLEFMA induces cell death via apoptotic pathway was provided by the *in vitro* experiments in H441 cells. The canonical intrinsic apoptosis is initiated by caspase-9 that cleaves procaspase-3 and procaspase-7, the cleaved and activated forms of which, in turn, cleave several other cellular targets, including PARP. Intact PARP participates in DNA repair mechanisms; however, its caspase-mediated cleavage inactivates it and forces cells towards programmed cell death. While apoptotic cell death is a hallmark of successful chemotherapy, by inhibiting the clonogenic cell survival CLEFMA demonstrated the ability to stop a cell from proliferating indefinitely, thereby eliminating the possibility of drug-resistant cancer stem cells forming a large colony.

In tumour tissue, the apoptotic effect of CLEFMA was manifested as the down-regulation of cell survival proteins

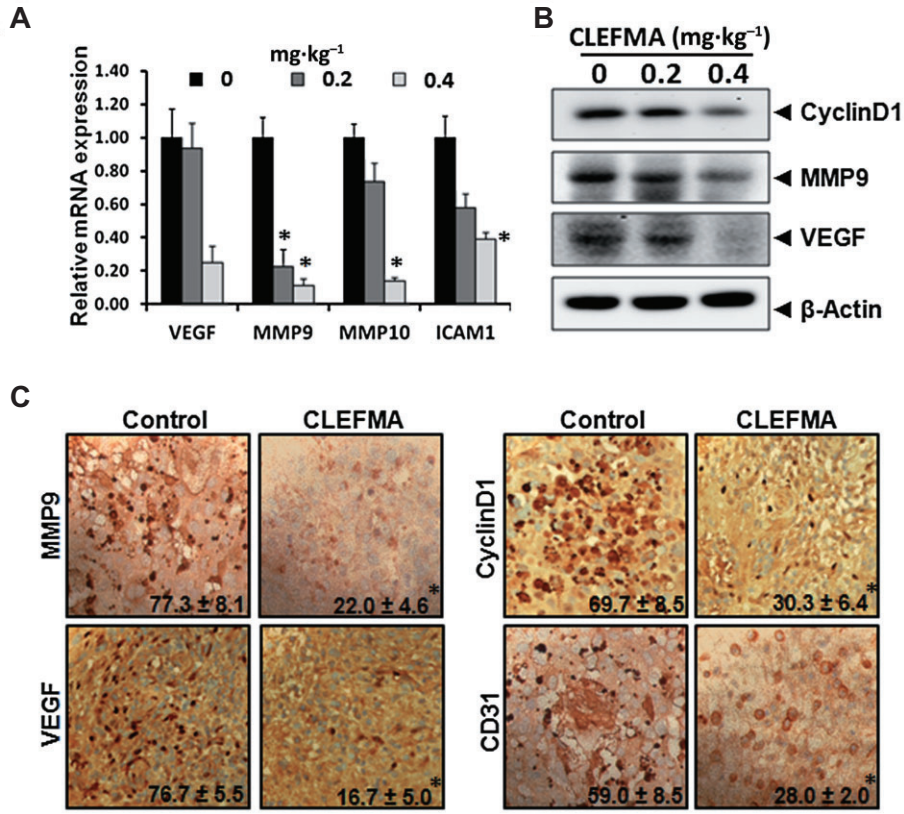


## Figure 7

CLEFMA suppresses the expression of the markers of tumour cell proliferation, invasion and angiogenesis in lung cancer xenograft. (A) CLEFMA inhibited the mRNA expression of NF–κB-dependent gene products that regulate proliferation (cyclin D1), invasion (MMP9/10 and ICAM1) and angiogenesis (VEGF-A. *$P < 0.05$ significantly different from untreated tumours. (B) CLEFMA treatment suppressed the expression of cyclin D1, MMP9 and VEGF. (C) A representative IHC result is provided showing that CLEFMA (0.4 mg·kg$^{-1}$) treatment inhibited cyclin D1, MMP9, VEGF and CD31. The quantification of IHC positivity is expressed as mean ± SEM of triplicate assays. *$P < 0.05$ significantly different from untreated tumours). At least three tissues from each group were selected randomly for reverse transcription PCR, immunoblotting and IHC.

and up-regulation of apoptosis inducers (Figure 3). Survivin blocks the mitochondrial pathway of apoptosis by inhibiting caspases and is expressed at high levels in cancer cells, but is not present in differentiated normal cells (Nakahara *et al.*, 2007). The CLEFMA-induced apoptosis was also associated with disappearance of BID, perhaps because of the caspase-mediated cleavage, and induction of BAX. During apoptosis, BID can also be cleaved by granzyme B, calpains and cathepsins. The protease-cleaved BID migrates to mitochondria where it induces permeabilization of the outer mitochondrial membrane that is dependent on pro-apoptotic proteins, such as BAX (Billen *et al.*, 2008). The CLEFMA-induced apoptosis was also associated with p53 phosphorylation, which suggests it to be a p53-dependent process. To determine whether the CLEFMA-induced cell death was dependent on the activation of caspases or the inhibition of transcription activity, we treated H441 cells in culture with CLEFMA (10 μM) in the presence of pan-caspase inhibitor z-VAD (1–10 μM) and transcription inhibitor actinomycin D (AMD). We found that the viability of H441 cells was very sensitive to z-VAD or AMD alone, even at concentrations lower than those conventionally used in such experiments (Wang *et al.*, 2005; Luster *et al.*, 2009). The high sensitivity of H441 cells to z-VAD and AMD precluded us from drawing any firm conclusions on the sole dependence of CLEFMA-induced cytotoxicity on caspase activation or transcription inhibition.

One mechanism of tumour inhibition by natural and synthetic chalcones is through inhibiting NF-κB activation (Kasinski *et al.*, 2008; Yadav *et al.*, 2011). Our own recent work on a diphenyldifluoroketone EF24 confirmed that compounds of this class inhibit NF-κB (Vilekar *et al.*, 2012). In lung cancer development, a constitutive activation of NF-κB pathway is commonly encountered (Meylan *et al.*, 2009). Therefore, we investigated NF-κB and other NF-κB-regulated gene products in tumour tissues. The level of nuclear p65 correlates with NF-κB transcriptional activity (Maguire *et al.*, 2011), and the rate of NF-κB nuclear translocation is dependent on the PKA-mediated phosphorylation of p65 (King *et al.*, 2011). As such, the nuclear expression of NF-κB phospho-p65 is an early and frequent phenomenon in the pathogenesis of lung cancer (Tang *et al.*, 2006). CLEFMA treatment in mice not only inhibited the nuclear localization of phospho-p65 but also reduced the levels of NFKB1 transcripts. The NF-κB inhibitory effects of CLEFMA were also confirmed by determining the *in vitro* DNA-binding ability of NF-κB in H441 cells. Interestingly, CLEFMA showed no effect on NF-κB DNA

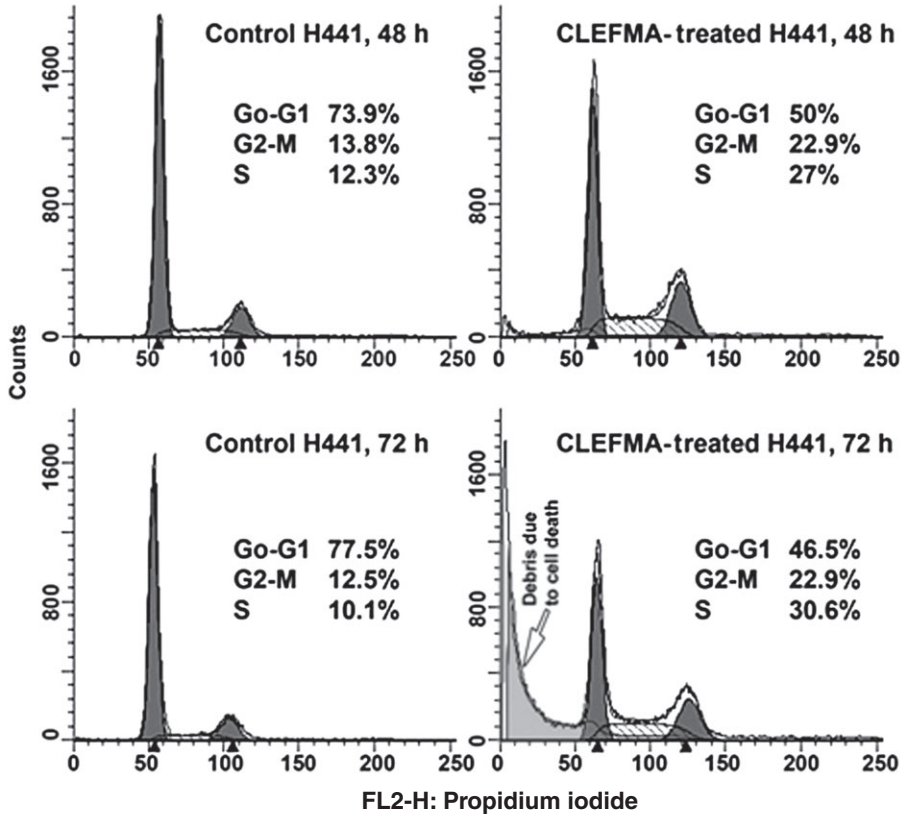


## Figure 8

CLEFMA treatment arrests H441 cells in S-phase of cell cycle. The data are representative set of more than three experiments. The insets provide the quantitation of cells in different phases of cell cycle as analysed by flow cytometry.

binding in the normal lung fibroblasts, CCL151. Earlier we have shown that CCL151 cells are resistant to CLEFMA-induced cell death (Sahoo *et al.*, 2012).

Further exploration of the key players in the NF-κB complex revealed an unexpected phenomenon. In normal circumstances, the phosphorylation of IκBα commits IκBα to its proteasome-mediated degradation pathway, releasing NF-κB to translocate into the nucleus and perform its transcriptional activity. However, in the present experiments, we observed that despite increased phosphorylation of IκBα, a large amount of phospho-IκBα was present in CLEFMA-treated H441 cells. Combined with the other observation that IKKα/β is also present in its activated/phosphorylated form, it appears that CLEFMA-induced NF-κB inhibition may not be dependent on the IKKα/β-IκBα interaction. Instead, we speculate that CLEFMA might be inhibiting the degradation of phospho-IκBα. We further hypothesize that the stabilization of IκBα–NF-κB complex prevents release, activation and/or nuclear translocation of NF-κB. The proteasome inhibitors are known to stabilize the phosphorylated form of IκBα that is still bound to NF-κB and prevent NF-κB activation (Traenckner *et al.*, 1994; McDade *et al.*, 1999). More recently, the proteasome inhibitors were found to increase the levels of cellular IκBα, which then translocate to the nucleus, associate with the nuclear p65 NF-κB, inhibit the NF-κB DNA-binding activity and induce apoptosis in prostate cancer cells (Vu *et al.*, 2008). Whether this phenomenon plays a part in CLEFMA-induced NF-κB inhibition would require further work in the context of H441 cells.

A critical step in the inflammatory pathway is the synthesis of $PGE_2$, catalysed by COX-2. Unlike COX-1, which is constitutively expressed in many cells and tissues, COX-2 is selectively induced by proinflammatory cytokines at the site of inflammation (Seibert and Masferrer, 1994). COX-2 overexpression is seen in many malignancies including adenocarcinoma and squamous cell carcinoma of the lung (Sandler and Dubinett, 2004) and specific inhibition of COX-2 was beneficial in clinical trials involving lung cancer (Mao *et al.*, 2011). Although the precise mechanisms responsible for the elevated COX-2 expression in lung cancer are not clear, such elevations are associated with poor clinical outcome and a forced expression of COX-2 enhances the survival of lung cancer cells (Brown and DuBois, 2004). We found that CLEFMA treatment in mice reduced the expression of COX-2 protein in a dose-dependent manner. Incidentally, NF-κB controls the transcription of COX-2 (Tsatsanis *et al.*, 2006; Wu, 2006). The other clinical prognosticators of NF-κB-mediated inflammation in non-small-cell lung cancer are the serum levels of circulating cytokines, such as TNF-α and IL-6 (De Vita *et al.*, 1998; Derin *et al.*, 2008; Su *et al.*, 2011). CLEFMA reduced the circulating levels of these proinflammatory cytokines in a significant manner. Together with NF-κB inhibition, the observations that CLEFMA reduced the serum levels of proinflammatory cytokines and suppressed COX-2

expression suggest that at least part of CLEFMA-induced suppression of tumour growth is mediated via its effect on the key mediators of inflammation.

In addition to the inflammation, NF-κB also plays a part in cell cycle progression, angiogenesis and cancer metastasis. The transcriptional regulation of a cell cycle proto-oncogene cyclin D1, which is required for G1-to-S transition during cell cycle, is under NF-κB control (Takebayashi *et al.*, 2003). The overexpression of cyclin D1 is associated with human tumourigenesis and cellular metastases (Fu *et al.*, 2004). CLEFMA treatment reduced the expression of cyclin D1 in tumour xenografts. Because cyclin D1 promotes the progression of cells through the G1-to-S phase of the cell cycle, its suppression is expected to cause a cell cycle arrest. Indeed, H441 cells showed a significant arrest in the S phase after CLEFMA treatment.

Apart from its effects on the cell cycle progression, CLEFMA also influenced angiogenesis and metastasis of cancer by modulating VEGF, MMPs and ICAM-1. These signalling molecules are also regulated by NF-κB (Chen *et al.*, 2011). The overexpression of VEGF, MMP and ICAM is associated with increased vascularization, poor prognosis and high-grade tumour metastasis in lung cancer (Fujimoto *et al.*, 1998; Lantuejoul *et al.*, 2003). These proteins play a critical role in cancer cell invasion and metastasis (Orlichenko and Radisky, 2008; Stetler-Stevenson, 2008). More evidence related to the anti-angiogenic effect of CLEFMA appeared from the reduced expression of CD31, which is a marker of ongoing angiogenesis and microvessel density in tumours. It is noteworthy that CD31 is also expressed on monocytes and granulocytes, and its reduced expression could also be a result of CLEFMA-induced reduction in inflammation and infiltration of monocytes and granulocytes in the tumour tissue. CLEFMA also down-regulated the levels of MMP9/10 and ICAM1, which are the factors involved in cell migration and adhesion. Overall, these results indicate that CLEFMA negatively influences angiogenic and metastatic potential of tumours.

In summary, the comprehensive *in vivo* results presented here extended our earlier observations on the anti-cancer effect of CLEFMA (Lagisetty *et al.*, 2010; Agashe *et al.*, 2011; Sahoo *et al.*, 2012). The pharmacological effects of CLEFMA include suppression of proinflammatory mediators and markers of invasion, angiogenesis and cell proliferation. The role of NF-κB inhibition appears to be pivotal in its action, but the exact mechanism of NF-κB inhibition remains to be established.

## Acknowledgement

The work was supported by National Institute of Health R03 CA143614-01.

## Conflict of interest

The authors state no conflict of interest.

## References

Agashe H, Sahoo K, Lagisetty P, Awasthi V (2011). Cyclodextrin-mediated entrapment of curcuminoid 4-[3,5-bis(2-chlorobenzylidene-4-oxo-piperidine-1-yl)-4-oxo-2-butenoic acid] or CLEFMA in liposomes for treatment of xenograft lung tumor in rats. Colloids Surf B Biointerfaces 84: 329–337.

Awasthi S, Brown K, King C, Awasthi V, Bondugula R (2011). A toll-like receptor-4-interacting surfactant protein-A-derived peptide suppresses tumor necrosis factor-alpha release from mouse JAWS II dendritic cells. J Pharmacol Exp Ther 336: 672–681.

Billen LP, Shamas-Din A, Andrews DW (2008). Bid: a Bax-like BH3 protein. Oncogene Suppl 1: S93–S104.

Brown JR, DuBois RN (2004). Cyclooxygenase as a target in lung cancer. Clin Cancer Res 10: 4266s–4269s.

Chaturvedi MM, Sung B, Yadav VR, Kannappan R, Aggarwal BB (2011). NF-kappaB addiction and its role in cancer: 'one size does not fit all'. Oncogene 30: 1615–1630.

Chen W, Li Z, Bai L, Lin Y (2011). NF-kappaB in lung cancer, a carcinogenesis mediator and a prevention and therapy target. Front Biosci 16: 1172–1185.

De Vita F, Orditura M, Auriemma A, Infusino S, Catalano G (1998). Serum concentrations of proinflammatory cytokines in advanced non small cell lung cancer patients. J Exp Clin Cancer Res 17: 413–417.

Derin D, Soydinc HO, Guney N, Tas F, Camlica H, Duranyildiz D *et al.* (2008). Serum levels of apoptosis biomarkers, survivin and TNF-alpha in nonsmall cell lung cancer. Lung Cancer 59: 240–245.

DiDonato JA, Mercurio F, Karin M (2012). NF-kappaB and the link between inflammation and cancer. Immunol Rev 246: 379–400.

Ferrara N (2002). VEGF and the quest for tumour angiogenesis factors. Nat Rev Cancer 2: 795–803.

Fu M, Wang C, Li Z, Sakamaki T, Pestell RG (2004). Minireview: cyclin D1: normal and abnormal functions. Endocrinology 145: 5439–5447.

Fujimoto K, Hosotani R, Wada M, Lee JU, Koshiba T, Miyamoto Y *et al.* (1998). Expression of two angiogenic factors, vascular endothelial growth factor and platelet-derived endothelial cell growth factor in human pancreatic cancer, and its relationship to angiogenesis. Eur J Cancer 34: 1439–1447.

Greten FR, Eckmann L, Greten TF, Park JM, Li ZW, Egan LJ *et al.* (2004). IKKbeta links inflammation and tumorigenesis in a mouse model of colitis-associated cancer. Cell 118: 285–296.

Himelstein BP, Canete-Soler R, Bernhard EJ, Dilks DW, Muschel RJ (1994). Metalloproteinases in tumor progression: the contribution of MMP-9. Invasion Metastasis 14: 246–258.

Hoffmann A, Xia Y, Verma IM (2007). Inflammatory tales of liver cancer. Cancer Cell 11: 99–101.

Karin M, Lawrence T, Nizet V (2006). Innate immunity gone awry: linking microbial infections to chronic inflammation and cancer. Cell 124: 823–835.

Kasinski AL, Du Y, Thomas SL, Zhao J, Sun SY, Khuri FR *et al.* (2008). Inhibition of IkappaB kinase-nuclear factor-kappaB signaling pathway by 3,5-bis(2-flurobenzylidene)piperidin-4-one (EF24), a novel monoketone analog of curcumin. Mol Pharmacol 74: 654–661.

Kilkenny C, Browne W, Cuthill IC, Emerson M, Altman DG (2010). Animal research: reporting *in vivo* experiments: the ARRIVE guidelines. Br J Pharmacol 160: 1577–1579.

Kim S, Takahashi H, Lin WW, Descargues P, Grivennikov S, Kim Y *et al.* (2009). Carcinoma-produced factors activate myeloid cells through TLR2 to stimulate metastasis. Nature 457: 102–106.

King CC, Sastri M, Chang P, Pennypacker J, Taylor SS (2011). The rate of NF-kappaB nuclear translocation is regulated by PKA and A kinase interacting protein 1. PLoS ONE 6: e18713.

Lagisetty P, Vilekar P, Sahoo K, Anant S, Awasthi V (2010). CLEFMA-an anti-proliferative curcuminoid from structure-activity relationship studies on 3,5-bis(benzylidene)-4-piperidones. Bioorg Med Chem 18: 6109–6120.

Lantuejoul S, Constantin B, Drabkin H, Brambilla C, Roche J, Brambilla E (2003). Expression of VEGF, semaphorin SEMA3F, and their common receptors neuropilins NP1 and NP2 in preinvasive bronchial lesions, lung tumours, and cell lines. J Pathol 200: 336–347.

Luster TA, Carrell JA, McCormick K, Sun D, Humphreys R (2009). Mapatumumab and lexatumumab induce apoptosis in TRAIL-R1 and TRAIL-R2 antibody-resistant NSCLC cell lines when treated in combination with bortezomib. Mol Cancer Ther 8: 292–302.

Maguire O, Collins C, O'Loughlin K, Miecznikowski J, Minderman H (2011). Quantifying nuclear p65 as a parameter for NF-kappaB activation: correlation between ImageStream cytometry, microscopy, and Western blot. Cytometry A 79: 461–469.

Mao JT, Roth MD, Fishbein MC, Aberle DR, Zhang ZF, Rao JY *et al.* (2011). Lung cancer chemoprevention with celecoxib in former smokers. Cancer Prev Res (Phila) 4: 984–993.

McDade TP, Perugini RA, Vittimberga FJ, Jr, Callery MP (1999). Ubiquitin-proteasome inhibition enhances apoptosis of human pancreatic cancer cells. Surgery 126: 371–377.

McGrath J, Drummond G, McLachlan E, Kilkenny C, Wainwright C (2010). Guidelines for reporting experiments involving animals: the ARRIVE guidelines. Br J Pharmacol 160: 1573–1576.

Meylan E, Dooley AL, Feldser DM, Shen L, Turk E, Ouyang C *et al.* (2009). Requirement for NF-kappaB signalling in a mouse model of lung adenocarcinoma. Nature 462: 104–107.

Nakahara T, Kita A, Yamanaka K, Mori M, Amino N, Takeuchi M *et al.* (2007). YM155, a novel small-molecule survivin suppressant, induces regression of established human hormone-refractory prostate tumor xenografts. Cancer Res 67: 8014–8021.

Orlichenko LS, Radisky DC (2008). Matrix metalloproteinases stimulate epithelial-mesenchymal transition during tumor development. Clin Exp Metastasis 25: 593–600.

Pikarsky E, Porat RM, Stein I, Abramovitch R, Amit S, Kasem S *et al.* (2004). NF-kappaB functions as a tumour promoter in inflammation-associated cancer. Nature 431: 461–466.

Sahoo K, Dozmorov MG, Anant S, Awasthi V (2012). The curcuminoid CLEFMA selectively induces cell death in H441 lung adenocarcinoma cells via oxidative stress. Invest New Drugs 30: 558–567.

Sandler AB, Dubinett SM (2004). COX-2 inhibition and lung cancer. Semin Oncol 31: 45–52.

Seibert K, Masferrer JL (1994). Role of inducible cyclooxygenase (cox-2) in inflammation. Receptor 4: 17–23.

Stathopoulos GT, Sherrill TP, Han W, Sadikot RT, Yull FE, Blackwell TS *et al.* (2008). Host nuclear factor-kappaB activation potentiates lung cancer metastasis. Mol Cancer Res 6: 364–371.

Stetler-Stevenson WG (2008). The tumor microenvironment: regulation by MMP-independent effects of tissue inhibitor of metalloproteinases-2. Cancer Metastasis Rev 27: 57–66.

Su C, Zhou C, Zhou S, Xu J (2011). Serum cytokine levels in patients with advanced non-small cell lung cancer: correlation with treatment response and survival. Med Oncol 28: 1453–1457.

Sunaga N, Shames DS, Girard L, Peyton M, Larsen JE, Imai H *et al.* (2011). Knockdown of oncogenic KRAS in non-small cell lung cancers suppresses tumor growth and sensitizes tumor cells to targeted therapy. Mol Cancer Ther 10: 336–346.

Takebayashi T, Higashi H, Sudo H, Ozawa H, Suzuki E, Shirado O *et al.* (2003). NF-kappa B-dependent induction of cyclin D1 by retinoblastoma protein (pRB) family proteins and tumor-derived pRB mutants. J Biol Chem 278: 14897–14905.

Tang X, Liu D, Shishodia S, Ozburn N, Behrens C, Lee JJ *et al.* (2006). Nuclear factor-kappaB (NF-kappaB) is frequently expressed in lung cancer and preneoplastic lesions. Cancer 107: 2637–2646.

Tili E, Michaille JJ, Wernicke D, Alder H, Costinean S, Volinia S *et al.* (2011). Mutator activity induced by microRNA-155 (miR-155) links inflammation and cancer. Proc Natl Acad Sci U S A 108: 4908–4913.

Traenckner EB, Wilk S, Baeuerle PA (1994). A proteasome inhibitor prevents activation of NF-kappa B and stabilizes a newly phosphorylated form of I kappa B-alpha that is still bound to NF-kappa B. EMBO J 13: 5433–5441.

Tsatsanis C, Androulidaki A, Venihaki M, Margioris AN (2006). Signalling networks regulating cyclooxygenase-2. Int J Biochem Cell Biol 38: 1654–1661.

Vendramini-Costa DB, Carvalho JE (2012). Molecular link mechanisms between inflammation and cancer. Curr Pharm Des 18: 3831–3852.

Vilekar P, Awasthi S, Natarajan A, Anant S, Awasthi V (2012). EF24 suppresses maturation and inflammatory response in dendritic cells. Int Immunol 24: 455–464.

Vu HY, Juvekar A, Ghosh C, Ramaswami S, Le DH, Vancurova I (2008). Proteasome inhibitors induce apoptosis of prostate cancer cells by inducing nuclear translocation of IkappaBalpha. Arch Biochem Biophys 475: 156–163.

Wang G, Guo X, Floros J (2005). Differences in the translation efficiency and mRNA stability mediated by 5′-UTR splice variants of human SP-A1 and SP-A2 genes. Am J Physiol Lung Cell Mol Physiol 289: L497–L508.

Wu KK (2006). Transcription-based COX-2 inhibition: a therapeutic strategy. Thromb Haemost 96: 417–422.

Wu W, O'Reilly MS, Langley RR, Tsan RZ, Baker CH, Bekele N *et al.* (2007). Expression of epidermal growth factor (EGF)/transforming growth factor-alpha by human lung cancer cells determines their response to EGF receptor tyrosine kinase inhibition in the lungs of mice. Mol Cancer Ther 6: 2652–2663.

Yadav VR, Prasad S, Sung B, Aggarwal BB (2011). The role of chalcones in suppression of NF-kappaB-mediated inflammation and cancer. Int Immunopharmacol 11: 295–309.

Yadav VR, Prasad S, Aggarwal BB (2012a). Cardamonin sensitizes tumour cells to TRAIL through ROS- and CHOP-mediated up-regulation of death receptors and down-regulation of survival proteins. Br J Pharmacol 165: 741–753.

Yadav VR, Prasad S, Sung B, Gelovani JG, Guha S, Krishnan S *et al.* (2012b). Boswellic acid inhibits growth and metastasis of human colorectal cancer in orthotopic mouse model by downregulating inflammatory, proliferative, invasive and angiogenic biomarkers. Int J Cancer 130: 2176–2184.